THE JOURNAL OF PHYSICAL CHEMISTRY Letters

Letter

Cite This: J. Phys. Chem. Lett. 2019, 10, 2775−2781

pubs.acs.org/JPCL

Multiphoton Excitation of $CsPbBr_3$ Perovskite Quantum Dots (PQDs): How Many Electrons Can One PQD Donate to Multiple Molecular Acceptors?

Sadananda Mandal* and Nikolai V. Tkachenko*

Chemistry and Advanced Materials Group, Faculty of Engineering and Natural Science, Tampere University, Korkeakoulunkatu 8, 33720 Tampere, Finland

Supporting Information

ABSTRACT: Metastable multiexcitonic states (MESs) of semiconductor quantum dots can be involved in multielectron transfer reactions, which opens new perspectives in nanomaterials-based optoelectronic applications. Herein, we demonstrate the generation of a MES in $CsPbBr_3$ perovskite quantum dots (PQDs) and its dissociation dynamics through multiple electron transfers to molecular electron acceptors, anthraquinones (AQs), bound to the PQD surface by a carboxylic anchor. As many as 14 excitons are produced at an excitation density of roughly 220 μJ cm^{-2} without detectable PQD degradation. Addition of AQ results in the formation of PQD−AQ hybrids with excess of AQs (PQD:AQ ≈ 1:20), which opens the possibility of multielectron transfer acts from MES to AQs. We found that the electron transfer saturates after roughly five transfer acts and that the first electron transfer (ET) time constant is as short as 1 ps. However, each ET increases the Coulomb potential barrier for the next ET, which decreases the rate of ET, resulting in a saturation after five ETs.

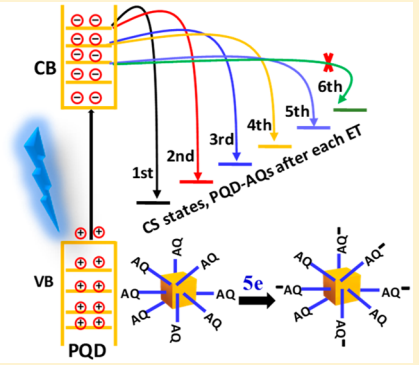

Multiexcitonic states (MESs) were observed recently in semiconductor quantum dots (QDs) and have been the subject of intense research interest, because they open new perspectives in designing photonic devices.[1−5] One can achieve multiple electron transfer (ET) reactions from a single QD for two reasons: (1) MESs are metastable, and (2) the energy of MESs can be much higher than that of the single-exciton state. MESs can be produced by direct multiexciton generation (MEG) in which absorption of a single photon with sufficiently high energy produces more than one exciton and the internal quantum efficiency (EQ) becomes greater than 100%. It is assumed that if photon energy (E_p) < band gap energy (E_g), EQ = 0; if $E_g < E_p < 2E_g$, EQ = 100% at maximum; but if $2E_g < E_p < 3E_g$, the EQ can be as high as 200%, and so on. Therefore, direct MEG, especially in the case of blue light absorbing QDs, can generate only a few excitons.[3] The generation of as many as seven excitons was reported for PbSe nanocrystal using excitation photon energy of $7.8E_g$,[3] but this value was considered to be overestimated because of photoionization in the presence of multiple excitons.[6,7] There are few more examples of direct MEG using a variety of QDs, including PbS,[8,9] PbSe,[10−12] CdSe,[13] InAs,[14−16] Ag_2S,[17] etc. Another practical way to generate multiexcitons in QDs is to photoexcite them with high excitation density.[1] In this case, absorption of more than one photon generates more than one exciton per QD. One can produce many excitons if the QD is photostable enough at higher excitation density. Zhu et al. reported the generation of 19 excitons in CdSe/CdS quasi-type II quantum dots by using high excitation density.[18]

To date, multiple exciton generation and dissociation of multiexcitonic states through charge transfer have been well studied for chalcogenide QDs. Recently, another class of semiconductor QDs, perovskite quantum dots (PQDs), have been considered as an alternative to chalcogenide QDs for their high quantum yields of emission and excellent solar energy conversion performance.[19−26] The carrier dynamics of PQDs is well-understood at the level of a single exciton,[27−30] whereas generation of multiexciton and recombination processes are still lacking. The extended functionalities of PQDs have been achieved by combining them with organic molecular electron donors and acceptors, preferably adsorbed on the surface of the PQDs to form ground-state complexes, and gaining photoinduced charge separation between PQDs and organic molecules.[31−36] To the best of our knowledge the possibility of charge transfer from PQD multiexcitonic states has not been demonstrated yet.

In our previous report, we showed that electron transfer from $CsPbBr_3$PQD to AQ is thermodynamically favorable because the conduction band (CB) energy of PQD (−3.0 eV relative to the vacuum level) is higher than the lowest unoccupied molecular orbital (LUMO) of AQ (−3.5 eV relative to vacuum level) and observed electron transfer with a time constant of 30 ps.[36] Herein, we report on the study of MESs in $CsPbBr_3$ PQDs and multiple electron transfer from

Received: April 12, 2019
Accepted: May 9, 2019
Published: May 9, 2019

DOI: 10.1021/acs.jpclett.9b01045
J. Phys. Chem. Lett. 2019, 10, 2775−2781

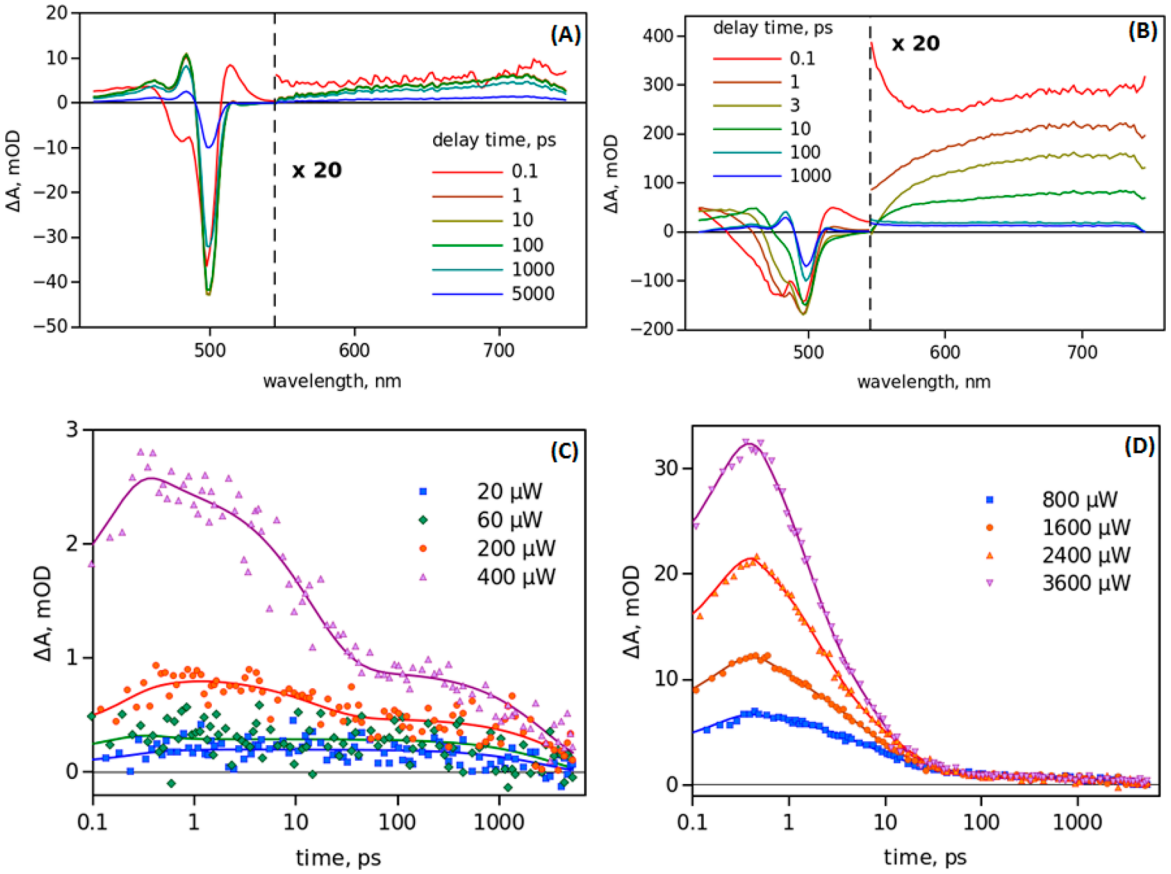

Figure 1. Time-resolved transient absorption spectra at a series of delay times at (A) low (60 μW) and (B) high (1600 μW) excitation intensities at 400 nm excitation. Spectra were corrected for group velocity dispersion. (C and D) Transient absorption decay profile at 720 nm with different excitation intensities as indicated in the plot at 400 nm excitation.

one multiexcited PQD to multiple electron acceptors, AQs in PQD−AQ hybrids, using ultrafast transient absorption (TA) spectroscopy. We show that as many as 14 excitons can be generated in one PQD at the highest excitation density used in this study and in the presence of AQ, 5 excitons are dissociated by electron transfer with the first electron-transfer reactions as fast as 1 ps. This result demonstrates the feasibility of using PQD-based nanohybrids as multielectron transferring light-harvesting and charge separation materials.

Details of materials, the experiment, and methods are given in the Supporting Information. The PQD−AQ complexes were prepared by a titration method as described in our previous publications.[36−38] In the case of PQD−AQ hybrids used in TA measurements, the PQD:AQ ratio was roughly 1:20 to ensure a sufficient number of electron acceptors were available in the medium. The PQDs were excited relatively close to the band gap at 470 nm and far from the band gap at 400 nm. The former allows working with relatively high concentrations, because at 470 nm, absorption of the PQD is roughly two times lower than at 400 nm. The latter has to be used to monitor the population of higher levels of the CB. To monitor the relative excitation density, the average excitation power was measured. This value is easy to measure, and it can be obtained with reasonably good accuracy. The power can be recalculated to the pulse energy (pulse repetition rate is 1 kHz), but calculation of the excitation energy density requires knowledge of the excitation spot size which presents the highest uncertainty in the excitation density estimation. The average excitation power varied within the range of 30−3600 μW. Taking a 1 mm^2 (roughly) excitation spot size, this corresponds to a 3−360 μJ cm^{-2} excitation density. We will use excitation average power as the measure of excitation energy density and will call it intensity throughout the text for brevity. For the analysis of the response dependence on excitation intensity, we will use a simple equation:

$$(I) = A_{\max}\left[1 - \exp\left(\frac{-I}{I_{\text{sat}}}\right)\right] \quad (1)$$

where I is the excitation intensity; $A(I)$ is the measured response, e.g., change in optical density at particular wavelength and delay time; $A_{\max}$ is the maximum possible change; and I_{sat} will be called saturation intensity, which corresponds to the photon density of one photon per PQD absorption cross section. In this case, excitation with I_{sat} results in excitation probability of $[1 - \exp(-1)] = 0.632$, or roughly 63%. The normalized absorption, emission, and emission decay of a PQD sample are shown in Figure S1. PQD has the lowest energy absorption peak at 497 nm (i.e., band gap at approximately 2.5 eV) and emission at 505 nm. The emission decay of the PQD was fitted with a single exponent, and the lifetime is 4.3 ns.

Multiexcitonic States in PQD. To investigate the MES, first we have analyzed the time-resolved transient absorption spectra of PQD at low (60 μW) and high (1600 μW) excitation intensities at 400 nm excitation (Figure 1A,B). At 60 μW excitation intensity, the maximum bleaching of the lowest-energy absorption band is roughly 44 mOD, which is roughly 15% of the steady-state absorption at this band. This indicates

DOI: 10.1021/acs.jpclett.9b01045
J. Phys. Chem. Lett. 2019, 10, 2775−2781

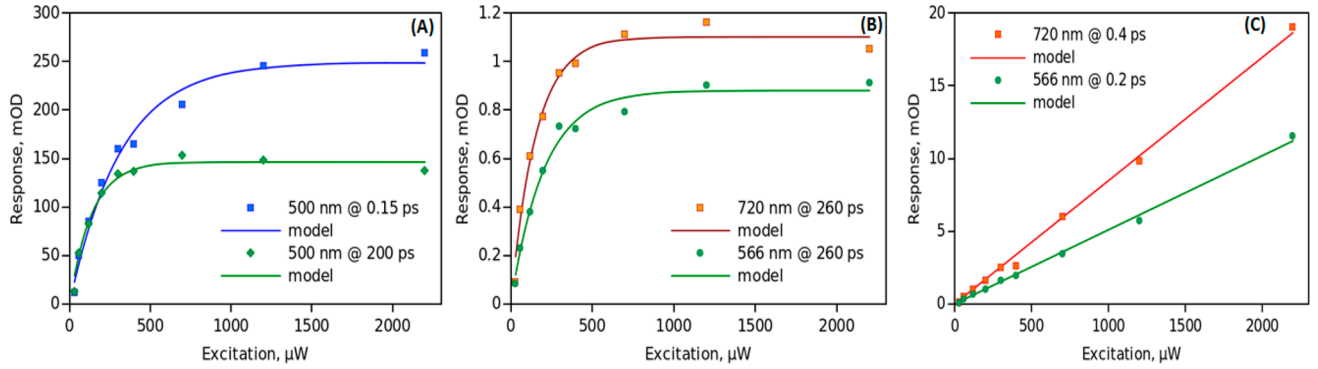

Figure 2. TA signal saturation of PQD with excitation at 470 nm (A) at 500 nm at two delay times, (B) at the red part of the spectrum at 260 ps delay, and (C) at the red part of the spectrum at short delay times.

that the probability of two-photon excitation is reasonably low. The transient absorption response at this excitation intensity is very simple after a fast (<1 ps) thermal relaxation. There is a bleaching of the lowest-energy absorption band near 500 nm; some increased absorption at 480 nm and shorter; and very broad and weak induced absorption in the red part of the spectrum (>550 nm), which becomes visible only after 20× magnification of this part of the spectrum. Gradual increase of the excitation intensity results in significant changes in the transient absorption response, which becomes much more complex. Ignoring the first picosecond thermal relaxation at short delay time (e.g., 1 ps), the ground-state absorption bleaching starts from the lowest energy band and extends to higher energy bands. With time, the bleached band becomes narrower through the recovery of the bleaching from the blue side of the spectrum. This can be explained qualitatively as follows: Multiphoton excitation promotes many electrons to the conduction band, which are filling energy levels from the bottom up. As long as there are excitons, the lowest conduction level is occupied and the band at 500 nm remains bleached. The higher levels are emptied first, and this is observed as faster bleaching recovery at the shorter wavelengths. At 100 ps delay time, the spectrum in this range is very much similar to the spectrum at the low excitation intensity.

The response in the red part of the spectrum is also very different at high excitation intensity. First, it is much stronger and it increases continuously with increased excitation. Similar to the blue part of the spectrum, most of the signal disappears in approximately a hundred picoseconds, and after this relaxation, the whole spectrum has a shape similar to that at low excitation intensity. It can be noted that the excitation was increased roughly 30 times, but bleaching at the 500 nm band is only 3.5 times stronger. Actually, it cannot be 30 times stronger because the ground-state absorption of the band is only 0.27, or only 6 times larger than the bleaching at 60 μW excitation intensity. It is clear that 1600 μW excitation saturates the bleaching at 500 nm, but absorption at this wavelength does not disappear completely and stays at the 45% level of the nonexcited sample.

The broad band absorption in the red part of the spectrum is most probably due to intraband absorption of the carriers in the CB. Thus, it can be used to monitor multiexciton excited states. The absorption decay profiles at 720 nm at different excitation intensities are presented in Figure 1C,D. Up to a hundred microwatt excitation intensity, the response is "flat", showing no decay until a few nanosecond delay time. At 200 μW excitation intensity, a faster decay can be noticed during the few tens of picoseconds after excitation, and this faster decay is very clear at 400 μW excitation intensity. Further increase of excitation intensity results in proportional increase of the response at a short delay time (e.g., 0.5 ps); a fast decay within a few tens of picosecond; and a weak signal at longer delay, which is virtually independent of the excitation intensity. Interestingly, the fast decay time is almost independent of the excitation intensity. The dependence of the signal intensity at 720 nm on the excitation intensity (at 400 nm) is shown in Figure S2 for two delay times, 0.4 and 200 ps. The first delay time corresponds roughly to the signal maximum intensity delay time, and the second delay time is selected after complete relaxation of the strong induced absorption at this wavelength. At the first delay time (0.4 ps), the signal increases linearly with the excitation intensity. At longer delay, the response intensity has clear saturation dependence, and its fit to eq 1 gives saturation intensity I_{sat} = 200 μW if the last points are excluded from the fit. We observed some sample degradation at high excitation intensity at 400 nm. The absorption of the lowest-energy band decreased by 6% and shifted to the blue by 1−2 nm (Figure S3), and there was a drop of the response signal at long delay for high excitation intensities (Figure S2B).

To reduce the degradation effect especially at higher excitation intensities, we shifted excitation closer to the band gap, at 470 nm. The transient absorption responses were essentially the same with both excitation wavelengths, though with 470 nm excitation the monitoring wavelength range was limited to 485−750 nm. The saturation dependence of the TA response was studied at various wavelengths and delay times (shown in Figure 2). Similar to the excitation at 400 nm, the TA response at short delay time in the red part of the spectrum increases linearly with excitation and it has typical saturation dependence at longer delay time and at 500 nm at any delay time. It is interesting to note that at the wavelength of 500 nm corresponding to the lowest energy level of the CB, the signal saturates faster at longer delay time than at the shorter, which can be viewed as biexciton at short delay versus one exciton at longer delay. The saturation dependence of TA response at 500 nm was fitted by using eq 1, and it gives the saturation intensities of 320 and 140 μW at 0.15 and 200 ps delays, respectively. If we assume that saturation of the signal at 500 nm takes place when the lowest conduction band level is fully occupied, e.g. populated with two electrons, then the saturation intensity of 320 μW corresponds to two-photon excitation on average. This agrees reasonably well with the single exciton state at longer delay, which saturates at 140 μW.

DOI: 10.1021/acs.jpclett.9b01045
J. Phys. Chem. Lett. 2019, 10, 2775−2781

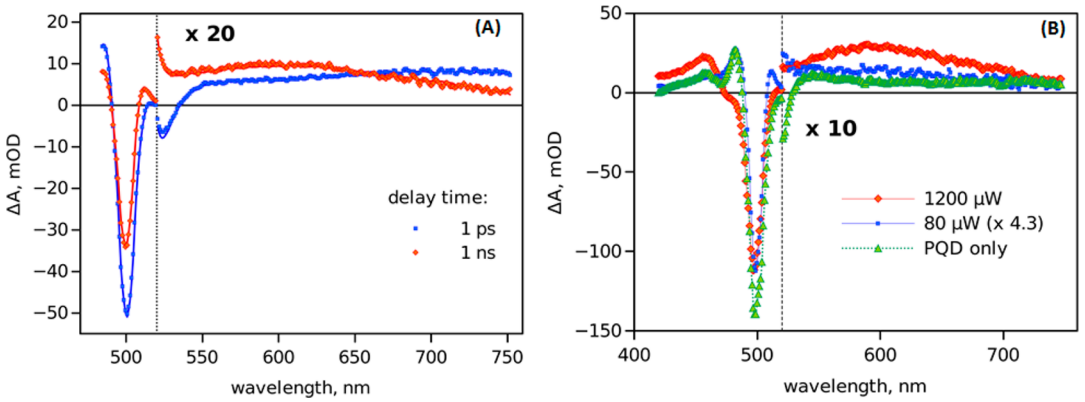

Figure 3. (A) TA spectra of PQD−AQ sample at two delay times obtained with 60 μW excitation intensity at 470 nm. (B) TA spectra at 1 ns delay time of PQD−AQ sample at higher excitation intensity (1200 μW) and low intensity (80 μW, multiplied by 4.3) and of pure PQD sample with the same 1200 μW excitation intensity at excitation wavelength of 400 nm.

Consequently, at the highest excitation intensity, the average number of populated levels in PQDs is 2200/320 = 7, which corresponds to the generation of 14 excitons.

It is also constructive to compare decay profiles at 500 and 720 nm for understanding the relaxation dynamics of MES, as presented in Figure S4. First, at a low excitation intensity (60 μW), the decay is fairly simple: there is virtually instant bleaching and slow recovery with a time constant in the nanosecond time domain. At the high excitation intensity shown, we expect the four lowest CB levels to be populated by electrons. The instant bleaching is stronger, and it is at the level of 85% of the ground-state absorption; it decays to roughly half of the ground-state absorption in a few tens of picoseconds, and the remaining part decays in much longer time scale of a few nanosecond, which is very close to the decay at low excitation intensity. At 720 nm the response is at its maximum at roughly 0.8 ps, but the signal starts to decay almost immediately, and the decay is smooth without any intermediate metastable state. However, this fast decay stops at roughly the 10% level in time roughly equal to the intermediate relaxation at 500 nm, and complete relaxation takes place simultaneously at all wavelengths with a few nanosecond time constant. The response at the red part can be taken as the measure of the total number of excitons. A qualitative explanation is that at the beginning, the average number of excitons per PQD is 8 in this case, and this multiexcitonic state has a short lifetime and decays to a relatively long-lasting monoexcitonic state in a few tens of picoseconds. At 720 nm, the decay is "smooth" as it shows the total number of excitons. At 500 nm, we monitor the population of the lowest-energy CB level, which does not change as long as there are at least two excitons in the PQD; therefore, there is no visible decay at 500 nm up to 10 ps delay. Then the biexcitonic state relaxes to the monoexcitonic state with time constant 20−30 ps, and the monoexciton decays to the ground state in a few nanoseconds.

Multiple Electron Transfer in PQD−AQ Hybrid. To investigate the multiple electron transfer from one PQD to multiple electron acceptors, AQ has been chosen as electron acceptors, and hence, PQD−AQ hybrids were prepared. Figure S5 shows the absorption, emission, and emission decays of different ratios of PQD−AQ hybrids. The absorption spectra of PQD remains unchanged after complex formation with AQ because the absorption intensities of AQ is much lower than that of PQD in the studied wavelength range. A remarkable emission quenching (more than 50%) of PQD was observed for 1:1 molar ratio of PQD:AQ, although the AQ is poorly soluble in toluene. This is an indication of complex formation between PQD and AQ through carboxylic acid binding groups, although the geometry of this complex, e.g., side or edge attachment of the AQ to PQD, cannot be determined. The relative emission quenching was quantitatively evaluated by employing Poisson statistics (Figure S4D) on ground-state complex formation and fitted result showed a very small (10%) mismatch between the experimental and model sample concentration ratio which is well within the experimental accuracy. Therefore, these results suggest efficient ground-state complex formation between PQD and AQ. In PQD−AQ hybrids, the emission and lifetime quenching of PQD are due to the electron transfer from PQD to AQ, which was already reported in our recent article.[36]

To observe the multiple electron transfer from an excited PQD to AQs, TA measurements of PQD−AQ hybrids were performed as a function of excitation intensities under the same conditions as those for PQDs. At low excitation (60 μW) intensities which can be qualified as monoexcitonic, the transient absorption is relatively simple and can be presented by two time-resolved spectra (excitation at 470 nm) at 1 ps and 1 ns, as shown in Figure 3A. The spectrum of the PQD−AQ sample at 1 ps delay time matches that of the pure PQD sample well, and this state can be assigned to the excited PQD; however, there is gradual change in the TA between 1 ps and roughly 100 ps in the range of 510−750 nm. At 1 ns delay time, the spectrum shows a broad absorption band in the range of 530−700 nm, which has intensity higher than that of the excited PQD in the range of 550−640 nm. The change can be observed as the absorption rise at the latter range, as illustrated in Figure S6. This broad band is attributed to the AQ anion, AQ^{-}.

There is one other distinctive spectral feature of this charge-transfer (CT) state, a sharp peak at 512 nm, which has a roughly 8-fold higher intensity than a broad band around 600 nm. This feature comes most probably from the PQD cation.

At a higher excitation intensity limit, the band around 600 nm increases in intensity, but there is noticeable change in the TA spectrum at shorter wavelengths, which is illustrated in Figure 3B showing TA spectra at 1 ns. The same figure present the TA spectrum of a pure PQD sample obtained with the same excitation intensity. As demonstrated above, the 1 ns delay time is sufficiently long to exclude any multiexcitonic states, meaning that the differences must come from different

DOI: 10.1021/acs.jpclett.9b01045
J. Phys. Chem. Lett. 2019, 10, 2775−2781

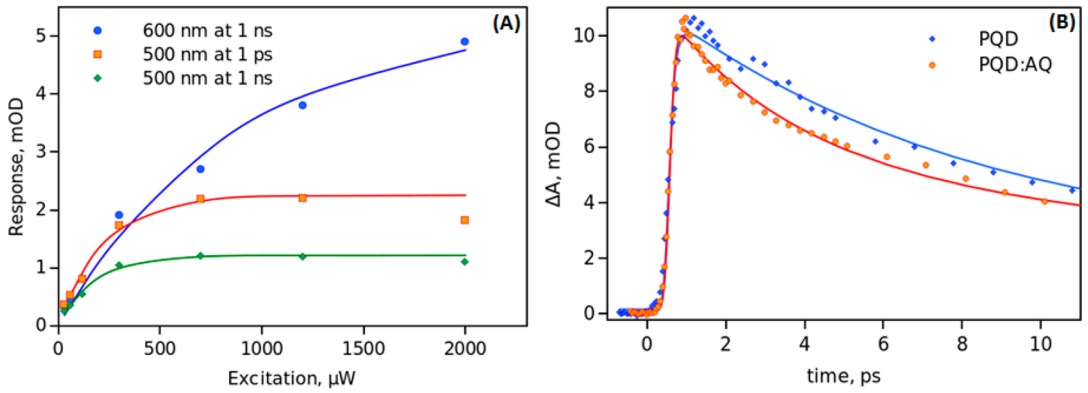

Figure 4. (A) Excitation intensity dependences of the PQD−AQ sample TA responses at a few selected wavelengths and delay times. Responses at 500 nm were divided by 100 to fit the scale. (B) Transient decay profiles of samples with and without AQ at 740 nm and excitation intensity of 1200 μW at 470 nm.

Scheme 1. Schematic Presentation of the Multiple ET Process

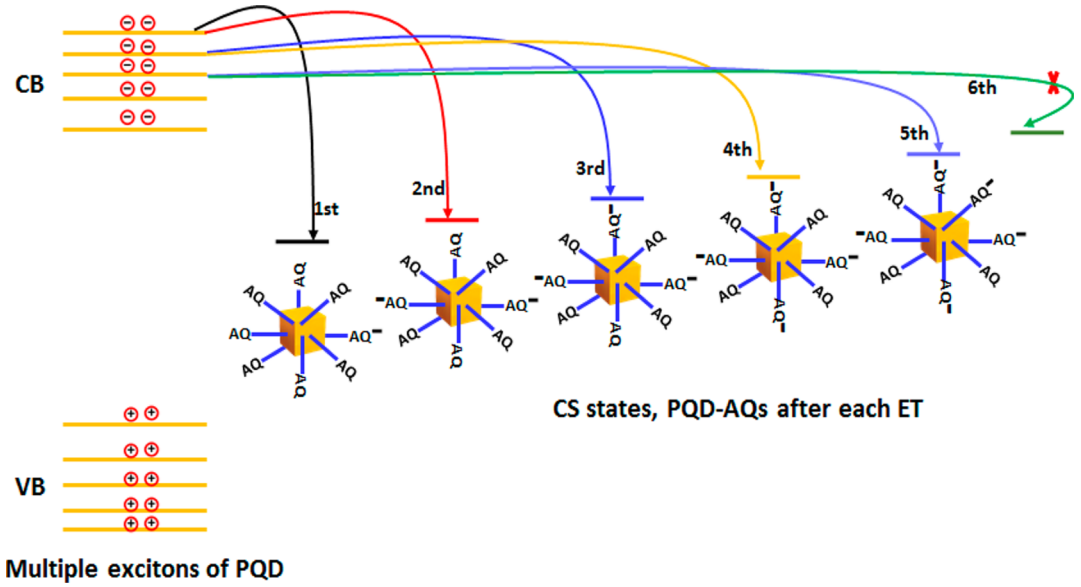

CT states. The analysis of the TA data at high excitation intensities is complicated by the CB electron absorption in the red part of the spectrum which increases linearly with the excitation intensity. This does not change after adding AQ, and at short delay times, we observed the same linear increase of the TA response with excitation intensity, as presented in Figure S7. Apparently the response due to AQ^- does not increase as fast as that of the multiexcitonic state, and no rise due to formation of AQ^- can be observed starting from an excitation intensity of a few hundred microwatts.

The dependence of the TA responses at 500 and 600 nm of PQD−AQ samples on excitation density at 470 nm is presented in Figure 4A. The responses at 600 nm present real signal amplitude and at 500 nm were divided by 100, which gives roughly the same initial slope of the dependence at low excitation intensities. This shows that although there is a saturation of the signal at 600 nm at 1 ns delay, it comes not as fast as at 500 nm. Using eq 1, the fitted result gives saturation intensity of 180 μW at 500 nm (1 ns) and 870 μW at 600 nm. If saturation intensity of 180 μW is attributed to the single-exciton case, then we conclude that with multiexciton excitation as many as on average 5 (870/180) electrons can be transferred to multiple molecular electron acceptors attached to single PQD with a single pulse excitation.

The number of electron transfers per PQD to AQ has also been evaluated based on the concentration of the AQ radical anion formed. The molar absorption coefficient of PQD at roughly 497 nm is 3.5×10^6 M^{-1} cm^{-1},[39,40] and the calculated concentration is 0.43×10^{-6} M. The concentration of the AQ radical anion at excitation intensity of 2200 μW is about 2.27×10^{-6} M (molar absorption coefficient of AQ radical anion at 600 nm is 11×10^3 M^{-1} cm^{-1}).[41] Therefore, the number of electron transfers per PQD is 5.2 (detailed calculation is given in the Supporting Information), which matches well with the calculation based on saturation intensity.

The electron transfer time constant of multiexcitonic states was evaluated by comparing transient absorption decay profiles (shown in Figure 4B) at 740 nm of PQDs and PQD−AQ hybrids with excitation intensity of 1200 μW. At this wavelength, the response is determined by the number of excitons in PQD predominantly. The excitation intensity selected for the comparison is high enough to guarantee generation of a multiexcitonic state. Our estimation suggests that a single excitation pulse creates 8−14 excitons (discussed above). In the presence of AQs, the rate of exciton relaxation

DOI: 10.1021/acs.jpclett.9b01045
J. Phys. Chem. Lett. 2019, 10, 2775−2781

increases, but the difference is relatively minor. At 1200 μW excitation intensity, the estimated number of AQ anions formed per PQD is roughly 3. Therefore, three out of eight excitons are dissociated by electron transfer and the remaining five excitons relax without generating an anion. Thus, one can expect only <40% faster exciton relaxation in the presence of AQs, which agrees with the decay differences presented in Figure 4B.

One can notice that the most essential difference is observed within 1−3 ps delay time; but after 3 ps delay time, the difference between two decays remains virtually in the same proportion, though at 3 ps only 30% of excitons have relaxed. This observation deserves a more careful consideration. It is clear that the driving force for the electron transfer is high for the electrons at higher levels, or for higher energy excitons. Therefore, at higher excitation intensity the first electron must be transferred to one of the AQs faster. However, the second electron transfer is expected to be slower because there is already positive charge (hole) on the PQD, which increases the Coulomb potential. Assuming the center-to-center distance is 4−5 nm and a nonpolar medium, a rough estimation of the added Coulomb potential after each electron transfer can be as large as 0.1 eV. This energy is close to the energy level spacing in the conduction band. If we assume that in the case of multiexcitonic state the first electron transfer takes place from the top of the exciton stack, after the first ET the driving force for the next ET is smaller for two reasons: the increased Coulomb potential and the lower energy of the next available exciton. After some number of ETs, the Coulomb potential outweighs other factors and no new ET takes place despite not all excitons having relaxed yet. This multiple electron-transfer process is presented in Scheme 1. A rough estimation for the ET of the multiexcitonic state is that it can be as short as within 1 ps, which is by an order in magnitude faster than the ET of the single-excitonic state.[31,36] However, quantitative estimation of the ET rates for multiexcitonic states requires thorough theoretical consideration of the ET dynamics, which differs essentially from the well-developed single-exciton case.

In summary, multiple excitons have been generated efficiently in $CsPbBr_3$ PQD using a high excitation density pulse. TA data analysis suggests that on an average 14 excitons per PQD can be generated by a single pulse excitation without noticeable sample degradation. It has also been demonstrated that the dissociation of multiexcitons is possible by electron transfer to multiple electron acceptors. As many as five electrons can be transferred from one multiexcited PQD to surface-attached electron acceptor AQs. The estimated time of ET of multiexcitonic states is as short as 1 ps, which is faster than the ET of a single excitonic state by an order in magnitude. Our finding opens up further prospects for the design of PQD-based multicomponent systems for photonic devices utilizing multiexcitons.

■ ASSOCIATED CONTENT

Supporting Information

The Supporting Information is available free of charge on the ACS Publications website at DOI: 10.1021/acs.jpclett.9b01045.

Materials and methods; absorption, emission, and emission decay of PQD; excitation intensity-dependent TA signal of PQD; TA decay profiles, absorption, emission, emission decays, and Poisson distribution of PQD−AQ; TA decay rise of PQD−AQ; excitation intensity-dependent TA signal of PQD−AQ; concentration calculation of AQ anion; and additional TA spectra of PQD and PQD−AQ at different excitation intensities (PDF)

■ AUTHOR INFORMATION

Corresponding Authors

*E-mail: sadananda.mandal@tuni.fi, sadtin.mandal@gmail.com (S.M.).

*E-mail: nikolai.tkachenko@tuni.fi (N.V.T).

ORCID

Sadananda Mandal: 0000-0002-4368-7047

Nikolai V. Tkachenko: 0000-0002-8504-2335

Notes

The authors declare no competing financial interest.

■ ACKNOWLEDGMENTS

S.M. is grateful to the TUT postdoctoral programme, Tampere University, Finland for financial support. The work is also a part of the Academy of Finland Flagship Programme, Photonics Research and Innovation (PREIN).

■ REFERENCES

(1) Klimov, V. I.; Mikhailovsky, A. A.; McBranch, D. W.; Leatherdale, C. A.; Bawendi, M. G. Quantization of Multiparticle Auger Rates in Semiconductor Quantum Dots. *Science* **2000**, *287*, 1011−1013.

(2) Schaller, R. D.; Klimov, V. I. High Efficiency Carrier Multiplication in PbSe Nanocrystals: Implications for Solar Energy Conversion. *Phys. Rev. Lett.* **2004**, *92*, 186601.

(3) Schaller, R. D.; Sykora, M.; Pietryga, J. M.; Klimov, V. I. Seven Excitons at a Cost of One: Redefining the Limits for Conversion Efficiency of Photons into Charge Carriers. *Nano Lett.* **2006**, *6*, 424−429.

(4) Nozik, A. J.; Beard, M. C.; Luther, J. M.; Law, M.; Ellingson, R. J.; Johnson, J. C. Semiconductor Quantum Dots and Quantum Dot Arrays and Applications of Multiple Exciton Generation to Third-Generation Photovoltaic Solar Cells. *Chem. Rev.* **2010**, *110*, 6873−6890.

(5) Beard, M. C. Multiple Exciton Generation in Semiconductor Quantum Dots. *J. Phys. Chem. Lett.* **2011**, *2*, 1282−1288.

(6) McGuire, J. A.; Sykora, M.; Joo, J.; Pietryga, J. M.; Klimov, V. I. Apparent Versus True Carrier Multiplication Yields in Semiconductor Nanocrystals. *Nano Lett.* **2010**, *10*, 2049−2057.

(7) Nootz, G.; Padilha, L. A.; Levina, L.; Sukhovatkin, V.; Webster, S.; Brzozowski, L.; Sargent, E. H.; Hagan, D. J.; Van Stryland, E. W. Size Dependence of Carrier Dynamics and Carrier Multiplication in PbS Quantum Dots. *Phys. Rev. B: Condens. Matter Mater. Phys.* **2011**, *83*, 155302.

(8) Ellingson, R. J.; Beard, M. C.; Johnson, J. C.; Yu, P.; Micic, O. I.; Nozik, A. J.; Shabaev, A.; Efros, A. L. Highly Efficient Multiple Exciton Generation in Colloidal PbSe and PbS Quantum Dots. *Nano Lett.* **2005**, *5*, 865−871.

(9) Karki, K. J.; Ma, F.; Zheng, K.; Zidek, K.; Mousa, A.; Abdellah, M. A.; Messing, M. E.; Wallenberg, L. R.; Yartsev, A.; Pullerits, T. Multiple Exciton Generation in Nano-Crystals Revisited: Consistent Calculation of the Yield Based on Pump-Probe Spectroscopy. *Sci. Rep.* **2013**, *3*, 2287.

(10) Trinh, M. T.; Houtepen, A. J.; Schins, J. M.; Hanrath, T.; Piris, J.; Knulst, W.; Goossens, A. P. L. M.; Siebbeles, L. D. A. In Spite of Recent Doubts Carrier Multiplication Does Occur in PbSe Nanocrystals. *Nano Lett.* **2008**, *8*, 1713−1718.

(11) Ji, M.; Park, S.; Connor, S. T.; Mokari, T.; Cui, Y.; Gaffney, K. J. Efficient Multiple Exciton Generation Observed in Colloidal PbSe

DOI: 10.1021/acs.jpclett.9b01045
J. Phys. Chem. Lett. 2019, 10, 2775−2781

Quantum Dots with Temporally and Spectrally Resolved Intraband Excitation. *Nano Lett.* **2009**, *9*, 1217−1222.
(12) Cirloganu, C. M.; Padilha, L. A.; Lin, Q.; Makarov, N. S.; Velizhanin, K. A.; Luo, H.; Robel, I.; Pietryga, J. M.; Klimov, V. I. Enhanced Carrier Multiplication in Engineered Quasi-Type-II Quantum Dots. *Nat. Commun.* **2014**, *5*, 4148.
(13) Matylitsky, V. V.; Dworak, L.; Breus, V. V.; Basché, T.; Wachtveitl, J. Ultrafast Charge Separation in Multiexcited CdSe Quantum Dots Mediated by Adsorbed Electron Acceptors. *J. Am. Chem. Soc.* **2009**, *131*, 2424−2425.
(14) Pijpers, J. J. H.; Hendry, E.; Milder, M. T. W.; Fanciulli, R.; Savolainen, J.; Herek, J. L.; Vanmaekelbergh, D.; Ruhman, S.; Mocatta, D.; Oron, D.; et al. Carrier Multiplication and Its Reduction by Photodoping in Colloidal In As Quantum Dots. *J. Phys. Chem. C* **2007**, *111*, 4146−4152.
(15) Pijpers, J. J. H.; Milder, M. T. W.; Delerue, C.; Bonn, M. (Multi)Exciton Dynamics and Exciton Polarizability in Colloidal In As Quantum Dots. *J. Phys. Chem. C* **2010**, *114*, 6318−6324.
(16) Schaller, R. D.; Pietryga, J. M.; Klimov, V. I. Carrier Multiplication in In As Nanocrystal Quantum Dots with an Onset Defined by the Energy Conservation Limit. *Nano Lett.* **2007**, *7*, 3469−3476.
(17) Sun, J.; Yu, W.; Usman, A.; Isimjan, T. T.; DGobbo, S.; Alarousu, E.; Takanabe, K.; Mohammed, O. F. Generation of Multiple Excitons in Ag_2S Quantum Dots: Single High-Energy versus Multiple-Photon Excitation. *J. Phys. Chem. Lett.* **2014**, *5*, 659−665.
(18) Zhu, H.; Song, N.; Rodríguez-Córdoba, W.; Lian, T. Wave Function Engineering for Efficient Extraction of up to Nineteen Electrons from One CdSe/CdS Quasi-Type II Quantum Dot. *J. Am. Chem. Soc.* **2012**, *134*, 4250−4257.
(19) Green, M. A.; Emery, K.; Hishikawa, Y.; Warta, W.; Dunlop, E. D. Solar Cell Efficiency Tables (Version 46). In *Progress in Photovoltaics: Research and Applications*; American Chemical Society, June 2015; pp 805−812.
(20) Nam, J. K.; Chai, S. U.; Cha, W.; Choi, Y. J.; Kim, W.; Jung, M. S.; Kwon, J.; Kim, D.; Park, J. H. Potassium Incorporation for Enhanced Performance and Stability of Fully Inorganic Cesium Lead Halide Perovskite Solar Cells. *Nano Lett.* **2017**, *17*, 2028−2033.
(21) Liu, Q.; Wang, Y.; Sui, N.; Wang, Y.; Chi, X.; Wang, Q.; Chen, Y.; Ji, W.; Zou, L.; Zhang, H. Exciton Relaxation Dynamics in Photo-Excited $CsPbI_3$ Perovskite Nanocrystals. *Sci. Rep.* **2016**, *6*, 29442.
(22) Yettapu, G. R.; Talukdar, D.; Sarkar, S.; Swarnkar, A.; Nag, A.; Ghosh, P.; Mandal, P. Terahertz Conductivity within Colloidal $CsPbBr_3$ Perovskite Nanocrystals: Remarkably High Carrier Mobilities and Large Diffusion Lengths. *Nano Lett.* **2016**, *16*, 4838−4848.
(23) Liang, J.; Wang, C.; Wang, Y.; Xu, Z.; Lu, Z.; Ma, Y.; Zhu, H.; Hu, Y.; Xiao, C.; Yi, X.; et al. All-Inorganic Perovskite Solar Cells. *J. Am. Chem. Soc.* **2016**, *138*, 15829−15832.
(24) Zhu, Z.-Y.; Yang, Q.-Q.; Gao, L.-F.; Zhang, L.; Shi, A.-Y.; Sun, C.-L.; Wang, Q.; Zhang, H.-L. Solvent-Free Mechanosynthesis of Composition-Tunable Cesium Lead Halide Perovskite Quantum Dots. *J. Phys. Chem. Lett.* **2017**, *8*, 1610−1614.
(25) Makarov, N. S.; Guo, S.; Isaienko, O.; Liu, W.; Robel, I.; Klimov, V. I. Spectral and Dynamical Properties of Single Excitons, Biexcitons, and Trions in Cesium-Lead-Halide Perovskite Quantum Dots. *Nano Lett.* **2016**, *16*, 2349−2362.
(26) Parobek, D.; Dong, Y.; Qiao, T.; Rossi, D.; Son, D. H. Photoinduced Anion Exchange in Cesium Lead Halide Perovskite Nanocrystals. *J. Am. Chem. Soc.* **2017**, *139*, 4358−4361.
(27) de Jong, E. M. L. D.; Yamashita, G.; Gomez, L.; Ashida, M.; Fujiwara, Y.; Gregorkiewicz, T. Multiexciton Lifetime in All-Inorganic $CsPbBr_3$ Perovskite Nanocrystals. *J. Phys. Chem. C* **2017**, *121*, 1941−1947.
(28) Li, B.; Huang, H.; Zhang, G.; Yang, C.; Guo, W.; Chen, R.; Qin, C.; Gao, Y.; Biju, V. P.; Rogach, A. L.; et al. Excitons and Biexciton Dynamics in Single $CsPbBr_3$ Perovskite Quantum Dots. *J. Phys. Chem. Lett.* **2018**, *9*, 6934−6940.
(29) Mondal, N.; De, A.; Das, S.; Paul, S.; Samanta, A. Ultrafast Carrier Dynamics of Metal Halide Perovskite Nanocrystals and Perovskite-Composites. *Nanoscale*, in press, DOI: 10.1039/C9NR01745C.
(30) Castañeda, J. A.; Nagamine, G.; Yassitepe, E.; Bonato, L. G.; Voznyy, O.; Hoogland, S.; Nogueira, A. F.; Sargent, E. H.; Cruz, C. H. B.; Padilha, L. A. Efficient Biexciton Interaction in Perovskite Quantum Dots Under Weak and Strong Confinement. *ACS Nano* **2016**, *10*, 8603−8609.
(31) Wu, K.; Liang, G.; Shang, Q.; Ren, Y.; Kong, D.; Lian, T. Ultrafast Interfacial Electron and Hole Transfer from $CsPbBr_3$ Perovskite Quantum Dots. *J. Am. Chem. Soc.* **2015**, *137*, 12792−12795.
(32) Maity, P.; Dana, J.; Ghosh, H. N. Multiple Charge Transfer Dynamics in Colloidal CsPbBr3 Perovskite Quantum Dots Sensitized Molecular Adsorbate. *J. Phys. Chem. C* **2016**, *120*, 18348−18354.
(33) De, A.; Mondal, N.; Samanta, A. Hole Transfer Dynamics from Photoexcited Cesium Lead Halide Perovskite Nanocrystals: 1-Aminopyrene as Hole Acceptor. *J. Phys. Chem. C* **2018**, *122*, 13617−13623.
(34) Chen, K.; Deng, X.; Dodekatos, G.; Tüysüz, H. Photocatalytic Polymerization of 3,4-Ethylenedioxythiophene over Cesium Lead Iodide Perovskite Quantum Dots. *J. Am. Chem. Soc.* **2017**, *139*, 12267−12273.
(35) Zhu, R.; Gao, C.; Sun, T.; Shen, L.; Sun, D.; Li, X. Surface Decorating of CH3NH3PbBr3 Nanoparticles with the Chemically Adsorbed Perylenetetracarboxylic Diimide. *Langmuir* **2016**, *32*, 3294−3299.
(36) Mandal, S.; George, L.; Tkachenko, N. V. Charge Transfer Dynamics in CsPbBr3 Perovskite Quantum Dots-anthraquinone/Fullerene (C_{60}) Hybrids. *Nanoscale* **2019**, *11*, 862−869.
(37) Virkki, K.; Demir, S.; Lemmetyinen, H.; Tkachenko, N. V. Photoinduced Electron Transfer in CdSe/ZnS Quantum Dot-Fullerene Hybrids. *J. Phys. Chem. C* **2015**, *119*, 17561−17572.
(38) Mandal, S.; Garcia Iglesias, M.; Ince, M.; Torres, T.; Tkachenko, N. V. Photoinduced Energy Transfer in ZnCdSeS Quantum Dot-Phthalocyanines Hybrids. *ACS Omega.* **2018**, *3*, 10048−10057.
(39) Ravi, V. K.; Swarnkar, A.; Chakraborty, R.; Nag, A. Excellent Green but Less Impressive Blue Luminescence from $CsPbBr_3$ perovskite Nanocubes and Nanoplatelets. *Nanotechnology* **2016**, *27*, 325708.
(40) Ravi, V. K.; Markad, G. B.; Nag, A. Band Edge Energies and Excitonic Transition Probabilities of Colloidal $CsPbX_3$ (X = Cl, Br, I) Perovskite Nanocrystals. *ACS Energy Lett.* **2016**, *1*, 665−671.
(41) Wightman, R. M.; Cockrell, J. R.; Murray, R. W.; Burnett, J. N.; Jones, S. B. Protonation Kinetics and Mechanism for 1,8-Dihydroxyanthraquinone and Anthraquinone Anion Radicals in Dimethylformamide Solvent. *J. Am. Chem. Soc.* **1976**, *98*, 2562−2570.

DOI: 10.1021/acs.jpclett.9b01045
J. Phys. Chem. Lett. 2019, 10, 2775−2781